

Photonic quadrupole topological phases in zero-dimensional cavity with synthetic dimensions

Weixuan Zhang^{1,2} and Xiangdong Zhang^{1,2*}

¹Key Laboratory of advanced optoelectronic quantum architecture and measurements of Ministry of Education, School of Physics, Beijing Institute of Technology, 100081, Beijing, China;

²Beijing Key Laboratory of Nanophotonics & Ultrafine Optoelectronic Systems, Micro-nano Center, School of Physics, Beijing Institute of Technology, 100081, Beijing, China;

*Corresponding author, E-Mail address: zhangxd@bit.edu.cn

Quadrupole topological insulator, which supports robust corner states, has been recently demonstrated in two-dimensional (2D) spatial lattices. Here, we design the first photonic quadrupole topological insulator in fully synthetic spaces with the utilization of 0D optical cavity. The frequency and orbital angular momentum (OAM) of light are used to form the 2D synthetic spaces. Four degenerate polarization states are mapped to the internal lattice sites within the unit cell. By suitably engineering the coupling between cavity modes with different frequencies, OAMs and polarizations, the ideal synthetic quadrupole topological insulators are obtained. By using the robust synthetic corner state, we present the possibility for achieving topological protection of multi-photon entangled states. Our designed synthetic photonic quadrupole topological insulators propose a unique platform to investigate higher-order topological phases in 0D system and possess potential applications in quantum information and communications.

The exploration of topological physics in both solid materials^{1,2} and classical waves systems³⁻⁶ has become one of the most fascinating frontiers in recent years. Based on the bulk-boundary correspondence principle, most of the D -dimensional topological systems studied so far are always featured by the $(D-1)$ -dimensional boundary state⁷⁻²². Recently, a new class of symmetry-protected higher-order topological insulators that possess lower-dimensional boundary states and obey a generalization of the standard bulk-boundary correspondence have been introduced²³⁻³⁵. One example is given by

the quadrupole topological insulator, which can exhibit ($D-2$)-dimensional topological states protected by the quantized bulk quadrupole polarization. Motivated by this novel property, many experimental implementations of the $2D$ quadrupole topological phase with $0D$ corner states have been realized in microwave³⁶, phononic³⁷, photonics³⁸ and electrical circuit systems³⁹. However, the designed structures typically have complex geometries in $2D$ real spaces. This makes the realization of multipole topological phases in higher-dimensional spaces become extremely difficult. Consequently, achieving quadrupole topological phases in a simple and even lower-dimensional system is needed to be explored.

On the other hand, except for the real physical dimensions, various degrees of freedom in photonic systems, such as frequency⁴⁰⁻⁴³, OAM^{44, 45} and external structural parameters⁴⁶⁻⁴⁹, are also able to be used to construct the synthetic space where the innovative light control and quantum information processing may be realized. Based on the synthetic dimension in photonics, we can also easily investigate higher-dimensional physics with lower-dimensional structures. For example, the Bloch oscillation in synthetic space along the frequency axis has been realized using a single dynamically modulated ring resonator⁵⁰. The effective magnetic field for photons in the $2D$ synthetic space is achieved in one optical cavity, where the topologically protected one-way edge state along the OAM- or frequency-axis appears⁵¹. In addition, the $3D$ topological phases, such as Weyl point and topological insulators, can be constructed using $2D$ systems with an auxiliary synthetic dimension⁵²⁻⁵⁴. Furthermore, some novel topological phenomena beyond $3D$, such as $4D$ quantum Hall effect, can also be implemented with the help of synthetic dimensions⁴⁸. It is therefore relevant to ask whether the synthetic dimensions can be used to construct the higher-order topological phases in the lower-dimensional space.

In this Letter, we design a photonic quadrupole topological insulator in synthetic $2D$ spaces with the utilization of dynamically modulated $0D$ optical cavity. The frequency and OAM of light are used to form a $2D$ synthetic space. Four polarization states are mapped to internal lattice sites within the unit cell. By using this synthetic corner state, we propose that the topological protection of multi-photon entangled

states may be achieved. Our work presents a new way to investigate higher-order topological phases in lower-dimensional system and possesses potential applications in quantum information and communications.

Results

Design of photonic quadrupole topological insulators with synthetic dimensions.

To design the synthetic quadrupole topological insulators, it is important to map different degrees of freedom in photonic systems to the actual tight-binding lattice model with quantized bulk quadrupole polarization. The general conceptual drawing is graphically shown in Fig. 1a. Here, the frequency and OAM of light are set as two-axes in synthetic spaces. Four linked polarization states with the same frequency and OAM are mapped to the intra-cell coupling condition (enclosed by the red dotted box). Four polarization angles used here are set as $\theta=0\text{deg}$ (purple site), 45deg (orange site), 90deg (red site) and 135deg (green site), respectively. Additionally, the connected lattice sites with different frequencies or OAMs represent the inter-cell couplings (enclosed by the black dotted box). By suitably designing the coupling strength between these states with different frequencies, OAMs and polarizations, the ideal quadrupole topological insulators in the synthetic space can be obtained.

In the following, we prove that the above proposed scheme can be actually realized with the utilization of $0D$ optical cavity. Here, the designed optical cavity should support a set of equally spaced resonant modes ($\omega_n=\omega_0+n\Omega$) when the dispersion effect is ignored. ω_0 is the frequency of the 0th mode, $\Omega=2\pi c/L\ll\omega_0$ is the free-spectral range of the optical cavity with the loop length being L . n is an integer marking the mode index in frequency axis. In addition, all optical elements in the cavity are chosen to have cylindrical symmetry, where the degenerated Laguerre-Gaussian modes with different radial (p) and azimuthal (l) indexes exist⁵¹. Moreover, each cavity mode with fixed OAM and frequency should possess four allowed polarization states ($\theta=0, 45, 90$ and 135deg). Hence, the electric field E in this optical cavity can be expanded as:

$$E = \sum_{l,n} \sum_{\theta}^{0,45,90,135} C_{l,n,\theta} A_{l,n,\theta}(r) e^{-il\phi} e^{i(\frac{\omega_n}{c}z - \omega_n t)}, \quad (1)$$

where $C_{l,n,\theta}$ is the amplitude for the cavity mode at frequency (ω_n), OAM (l) and polarization (θ). $A_{l,n,\theta}(r)$ is the corresponding modal profile perpendicular to the direction of beam propagation. ϕ denotes the azimuthal coordinate. These different cavity modes ($C_{l,n,\theta}$) can be mapped to the synthetic lattice sites in Fig. 1a. In this case, the synthetic quadrupole topological insulator is able to be created by suitably engineering the coupling strength between these cavity modes. To fulfill the ideal coupling configuration, the large optical cavity consisting of three parts (polarization cavity, OAM cavity and frequency cavity) is designed, as shown in Fig. 1b.

The intra-cell coupling within the synthetic lattice model can be achieved by using the designed polarization cavity (enclosed by the red dot box), where eight kinds of polarization conversions “0deg \rightleftharpoons 45deg \rightleftharpoons 90deg \rightleftharpoons 135deg \rightleftharpoons 0deg” with fixed frequency and OAM exist. For this requirement, eight loops in the designed polarization cavity (the same length L with the modal coupling phase being $e^{i\omega_n L/c} = e^{i\omega_0 L/c}$) are used to perform these transformations, respectively. We note that each loop contains the designed polarization selection (only specific polarization state can pass through) and rotation ($\theta \rightarrow \theta + 45\text{deg}$) operations, as marked by the colored triangles and squares, so that the required polarization conversion can be achieved. It is important to note that the negative intra-cell coupling should be introduced when the polarization conversion of “0deg \rightleftharpoons 135deg” is carried out. This can be easily achieved by adding a π phase delay (marked by yellow rectangles in Fig. 1b) in the specific cavity loop. Moreover, the reflectivity of beam splitters (BS) used here should be suitable engineered [$R(\text{BS}_1)=0.25$, $R(\text{BS}_2)=0.33$ and $R(\text{BS}_3)=0.5$] to make the absolute value of the allowed intra-cell coupling coefficients become identical.

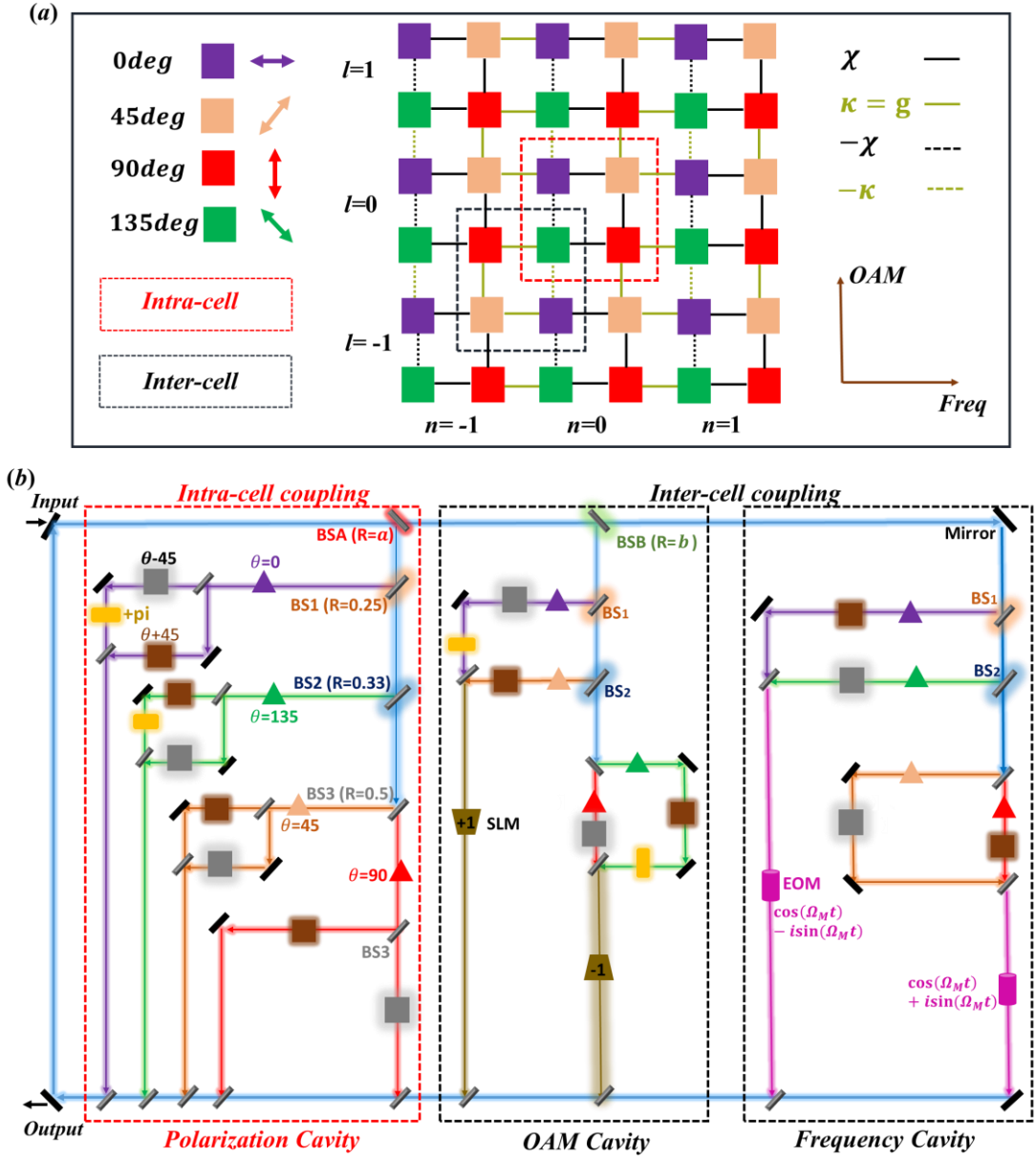


Figure 1 | Design of synthetic quadrupole topological insulator in zero-dimensional cavity. (a) The lattice model of quadrupole topological phases in synthetic 2D spaces. The frequency and OAM of light are set as two-axes in synthetic spaces. Four polarization states $\theta=0\text{deg}$, 45deg , 90deg and 135deg are considered as the internal lattice sites within the unit cell. The red and black dot boxes marked the intra- and inter-cell coupling conditions. (b) The designed 0D optical cavities, which include three cavities (polarization, OAM and frequency cavities), can realize the quadrupole topological insulator in synthetic spaces.

Based on the coupled mode theory, the change of the modal amplitude after each round-trip within the polarization cavity can be expressed as (the coupling phase $e^{i\omega_0 L/c}$ is a global phase, which can be neglected without loss of generality):

$$\begin{aligned}
\frac{d}{dt}c_{l,n,0} &= i\chi(c_{l,n,45} + e^{i\pi}c_{l,n,135}), & \frac{d}{dt}c_{l,n,45} &= i\chi(c_{l,n,90} + c_{l,n,0}), \\
\frac{d}{dt}c_{l,n,90} &= i\chi(c_{l,n,\theta,135} + c_{l,n,45}), & \frac{d}{dt}c_{l,n,135} &= i\chi(e^{i\pi}c_{l,n,0} + c_{l,n,90}),
\end{aligned} \tag{2}$$

where the value of coupling coefficient is expressed as $\chi=R(\text{BS}_A) * R(\text{BS}_1) * R(\text{BS}_3)=a/8$ (a is the reflectivity of the ‘BS_A’). It is clearly shown that our designed modal conversion configuration induced by the polarization cavity is identical to the intra-cell coupling of the lattice model with quantized bulk quadrupole polarization.

On the other hand, to introduce the appropriate inter-cell coupling between different unit cell in synthetic spaces, two other cavities with either OAM or frequency control are designed (enclosed by the black dot box in Fig. 1b). Firstly, we focus on the modal coupling with different OAM indexes (but the same frequency) by using a cavity (four loops) with OAM modulation. Here, the length of each loop is equal to be L so that the global coupling phase $e^{i\omega_0 L/c}$ can be neglected. To fulfill the ideal coupling between cavity modes with different OAMs, each loop should possess a spatial light modulator (SLM) with a broad bandwidth to change the OAM of light by either +1 or -1. In addition, each cavity loop also has engineered polarization control to achieve the required polarization conversions (0deg $\xrightarrow{l-1}$ 135deg, 135deg $\xrightarrow{l-1}$ 0deg, 45deg $\xrightarrow{l-1}$ 90deg and 90deg $\xrightarrow{l-1}$ 45deg). Also, a π phase delay is applied to introduce the negative inter-cell couplings for 0deg $\xrightarrow{l-1}$ 135deg and 135deg $\xrightarrow{l-1}$ 0deg. In this case, the variation of cavity modes with the light travelling a round-trip within the OAM cavity can be expressed as:

$$\begin{aligned}
\frac{d}{dt}c_{l,n,0} &= i\kappa e^{i\pi}c_{l+1,n,135}, & \frac{d}{dt}c_{l,n,45} &= i\kappa c_{l+1,n,90}, \\
\frac{d}{dt}c_{l,n,135} &= i\kappa e^{i\pi}c_{l-1,n,0}, & \frac{d}{dt}c_{l,n,90} &= i\kappa c_{l-1,n,45},
\end{aligned} \tag{3}$$

where the coupling coefficient can be expressed as $\kappa=[1-R(\text{BS}_A)] * R(\text{BS}_B) * R(\text{BS}_1)=(1-a)b/4$ (b is the reflectivity of ‘BS_B’).

Except for the modal coupling with different OAMs, the conversion between

cavity modes with different frequencies (but the same OAM) should also be achieved. For this requirement, the length of four loops in the frequency cavity should be equal to L (neglected global coupling phase $e^{i\omega L/c}$). Additionally, each loop possesses an electro-optic phase modulators (EOMs) to induce time-dependent transmissions⁵⁰⁻⁵³. There are two different transmission coefficients induced by EOMs, which can be expressed as: $T = e^{i\beta[\cos(\Omega_M t) \pm i \sin(\Omega_M t)]}$, where Ω_M is the modulation frequency and β denotes the modulation amplitude. In the presence of a travelling signal $e^{i\omega t}$, the transmitted wave can be expressed as: $T e^{i\omega t} \approx e^{i\omega t} + \beta e^{i(\omega \pm \Omega_M)t}$. It is clearly shown that the proposed EOM can change the modal frequency by either Ω_M or $-\Omega_M$. Combining this dynamically modal control and suitable polarization manipulations, the ideal inter-cell coupling along frequency dimension (0deg $\xrightarrow{l-1}$ 45deg, 135deg $\xrightarrow{l-1}$ 90deg, 45deg $\xrightarrow{l-1}$ 0deg and 90deg $\xrightarrow{l-1}$ 135deg) can be realized.

In the weak modulation regime and without the detuning of the modulation frequency from the free-spectral range of the cavity ($\Omega_M = \Omega$), the change of the modal amplitude after each round-trip with light passing through the EOM gives:

$$\begin{aligned} \frac{d}{dt} c_{l,n,0} &= ig c_{l,n-1,45}, & \frac{d}{dt} c_{l,n,135} &= ig c_{l,n-1,90}, \\ \frac{d}{dt} c_{l,n,45} &= ig c_{l,n+1,0}, & \frac{d}{dt} c_{l,n,90} &= ig c_{l,n+1,135}. \end{aligned} \quad (4)$$

Here, the coupling coefficient is expressed as $g = \beta[1-R(\text{BS}_A)][1-R(\text{BS}_B)]R(\text{BS}_1) = \beta(1-a)(1-b)/4$.

Combing the modal coupling relationship equations 1-3 within the designed cavity, the Hamiltonian of such a system can be expressed as:

$$\begin{aligned} H = & \sum_{n,l} g (a_{l,n-1,45}^+ a_{l,n,0} + a_{l,n-1,90}^+ a_{l,n,135} + a_{l,n+1,0}^+ a_{l,n,45} + a_{l,n+1,135}^+ a_{l,n,90}) \\ & + \kappa (a_{l+1,n,135}^+ a_{l,n,0} e^{i\pi} + a_{l+1,n,90}^+ a_{l,n,45} + a_{l-1,n,0}^+ a_{l,n,135} e^{i\pi} + a_{l-1,n,45}^+ a_{l,n,90}) \\ & + \chi (a_{l,n,45}^+ a_{l,n,0} + a_{l,n,90}^+ a_{l,n,45} + a_{l,n,135}^+ a_{l,n,90} + e^{i\pi} a_{l,n,0}^+ a_{l,n,135} \\ & + e^{i\pi} a_{l,n,135}^+ a_{l,n,0} + a_{l,n,0}^+ a_{l,n,45} + a_{l,n,45}^+ a_{l,n,90} + a_{l,n,90}^+ a_{l,n,135}), \end{aligned} \quad (5)$$

where we set $\hbar=1$. $a_{l,n,\theta}^+$ ($a_{l,n,\theta}$) is the creation (annihilation) operator for the cavity mode with frequency n , OAM l and polarization θ . The Hamiltonian in equation 4 presents the same form with that of the quadrupole topological insulator in real space^{24,25}. In following parts, we assume that inter-cell couplings along frequency and OAM axes are identical $g=\kappa$. This requires the modulation strength and reflectivity of ‘BS_B’ to satisfy $b=\beta/(1+\beta)$.

In order to exhibit the higher-order topological effect in our designed synthetic space, the artificial boundaries along both frequency and OAM axes should be included. This is not a trivial problem since the boundaries are not real. We can follow the previous work to introduce the frequency boundary by coupling with a secondary cavity as proposed in ref.⁵¹. And, the key of creating the OAM boundary is the design of holes in BSs, which is systematically analyzed in ref.⁴⁵. Actually, there are many factors limiting the size of the synthetic lattice, for example, the effective operation range of the optical elements. Here, we assume that frequency boundaries locate at $n=\pm 5$ and OAM boundaries are chosen as $l=0$ and $l=10$. In this case, the finite lattice model with open boundary condition is generated in the synthetic space where totally 484 sites (11 resonant frequencies, 11 OAMs and 4 polarizations) exist in this system. To illustrate the relationship between the topological property and the ratio between inter- and intra-cell coupling in synthetic dimensions, we plot the evolution of eigenspectrum of Hamiltonian (equation 4) with different values of g/χ (χ is normalized to be 1), as shown in Fig. 2a. For the practical realization of these different coupling relations, the reflectivities of “BS_A” and “BS_B” should be suitably adjusted. We find that there is neither edge nor corner state within the trivial bulk band gap when $g<\chi$ [$b<0.5a/(1-a)$]. And, the topological phase transition appears at the point with $g=\chi$ where the bulk band gap gets closed. Beyond the transition point ($g>\chi$), the bulk gap opens again. Then, both edge and midgap corner states appear. This can be further shown in Fig. 2b where the corresponding eigenvalues at $g=8$ [$b=4a/(1-a)$] are plotted. It is find that both fourfold degenerate ‘zero-energy’ corner states and gapped edge states exist in this topologically non-trivial band gap. To

clearly illustrate the midgap corner and edge states, in Fig. 2c and 2d, the distribution of the corner ($E=0$) and edge ($E=8$) states in the synthetic space are plotted. As expected, the eigenmode is highly localized at corners or edges within the finite lattice model in synthetic spaces that is the same as the actual quadrupole topological insulator in real spaces.

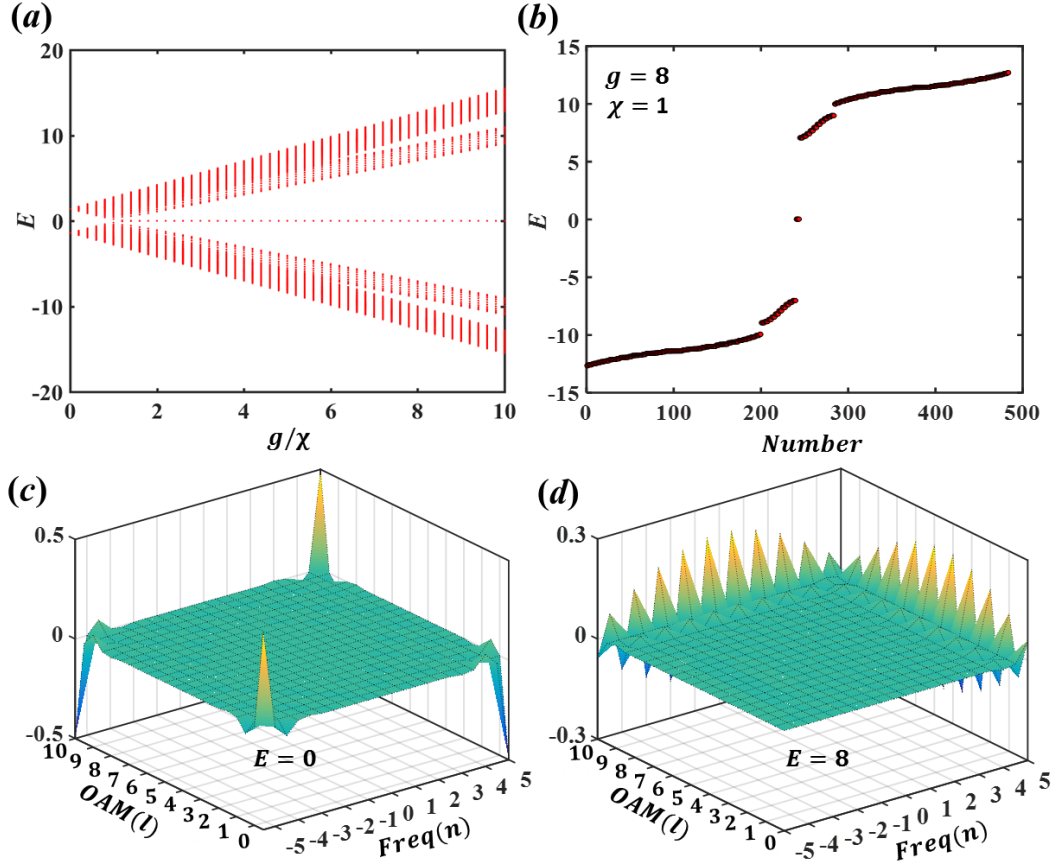


Figure 2 | Eigenspectrum and eigenmodes for the synthetic quadrupole topological insulator. (a) The evolution of eigenspectrum with different values of g/χ ($\chi=1$). (b) The eigenspectrum at $g=8$. (c) and (d) The modal distribution of corner and edge states in the synthetic space.

Topologically protected evolution of corner state in synthetic spaces. To characterize the evolution of corner and edge states in the synthetic space, we perform numerical simulation of output fields from the designed optical cavity. The general coupled-mode equations for our designed synthetic quadrupole topological insulators with the consideration of input and output ports can be expressed as:

$$\begin{aligned}
\frac{dc_{l,n,0}}{dt} &= -\gamma c_{l,n,0} - i\chi c_{l,n,45} + i\chi c_{l,n,135} - igc_{l,n-1,45}(1-\delta_{-5,n}) - i\kappa c_{l+1,n,135}(1-\delta_{10,l}) + \sqrt{\gamma} S_{l,n,0}^{in} \\
\frac{dc_{l,n,45}}{dt} &= -\gamma c_{l,n,45} - i\chi c_{l,n,0} - i\chi c_{l,n,90} - igc_{l,n+1,0}(1-\delta_{5,n}) - i\kappa c_{l+1,n,90}(1-\delta_{10,l}) \\
\frac{dc_{l,n,90}}{dt} &= -\gamma c_{l,n,90} - i\chi c_{l,n,45} - i\chi c_{l,n,135} - igc_{l,n+1,135}(1-\delta_{5,n}) - i\kappa c_{l-1,n,45}(1-\delta_{0,l}) \\
\frac{dc_{l,n,135}}{dt} &= -\gamma c_{l,n,135} - i\chi c_{l,n,90} + i\chi c_{l,n,0} - igc_{l,n-1,90}(1-\delta_{-5,n}) - i\kappa c_{l-1,n,0}(1-\delta_{0,l}) \\
S_{l,n,\theta}^{out} &= \sqrt{\gamma} c_{l,n,\theta} \quad ,
\end{aligned} \tag{6}$$

where $\gamma/2$ is the decay rate through the coupling between the optical cavity and the input-output channel. We assume that all cavity modes couple to the input-output channel with equal rates. $S_{l,n,\theta}^{in}$ ($S_{l,n,\theta}^{out}$) is the input (output) modal amplitude at frequency n , OAM l and polarization θ . The artificial boundary in the synthetic space is chosen as $n=\pm 5$, $l=0$ and $l=10$. Here, we only focus on the case that the polarization angle of input signal is 0deg. Similar results with other input polarizations are provided in the Supplementary Information.

In our simulations, we set the coupling rate between the input (and output) port and the optical cavity as $\gamma=0.1$. And, all other parameters are identical with those used in the calculation of eigenspectrum shown in Fig. 2a. To effectively excite the synthetic corner state, the input signal should locate at the corner (left-up) of the synthetic space. No corner excitation appears when the input state locates in the bulk of the synthetic space (see Supplementary Information). Figs. 3a-3c show the steady-state modal distribution with the value of $g(\chi)$ being 1(1), 2(1) and 8(1), respectively. The input signal is selected as $S_{10,-5,0}^{in} = e^{i0t}$ ('zero energy' excitation). We find that no corner localization appears when the coupling strength satisfied the relationship of $g=\chi$. This is due to the fact that no band gap exists in this case. While, with increasing the value of g/χ , the concentration of the output optical mode at the corner of the synthetic space appears. Additionally, the modal profile is completely the same as the midgap corner state, as shown in Fig. 2c. Moreover, the larger the value of g/χ is, the more significant localization appears at the corner of the synthetic space. If $g/\chi < 1$, corner states cannot be excited in the trivial band gap (see

Supplementary Information). Except for the corner excitation, the synthetic edge state can also be excited with suitable input signals (see Supplemental Information).

The most important property of the topologically-protected corner state is that it is robust with disorders. To illustrate this phenomena, we calculate the steady-state solution of the output field with significant disorders on g/χ at different lattice sites. The configuration average (10 times) is performed to eliminate the accidental result in the disorder system. The results are shown in Fig. 3d. We find that sharply localized output fields at the corner of the synthetic space still exist at zero energy when the values of $g(\chi)$ on different lattice sites are randomly selected ranging from 4(0.5) to 16(2). It clearly reveals the robustness of the corner state for the synthetic quadrupole topological insulator.

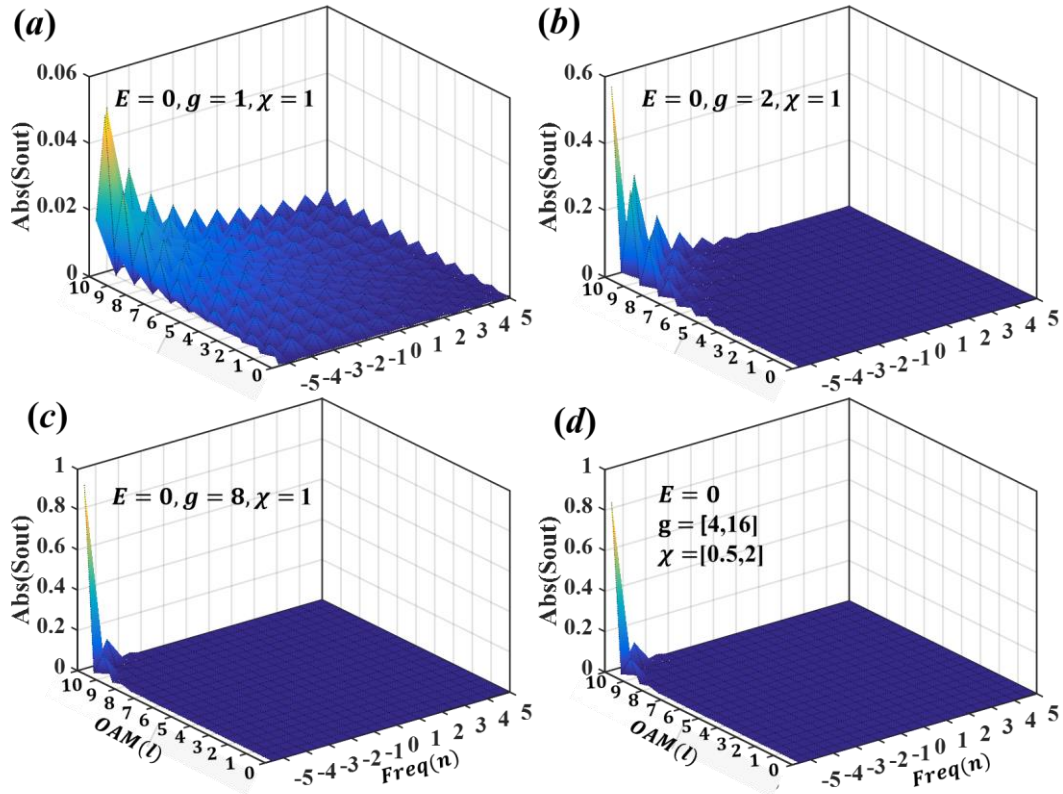


Figure 3 | Evolution of corner state in synthetic spaces. (a)-(c) The steady-state modal distribution with the value of $g(\chi)$ being 1(1), 2(1) and 8(1), respectively. (d) The steady-state modal distribution of corner state under the influence of disorder where $g(\chi)$ are randomly selected ranging from 4(0.5) to 16(2) between different lattice sites.

Topologically protection of multi-photon entangled states with synthetic corner

state. A fascinated potential application of our designed synthetic quadrupole topological insulator is the realization of topological protection of multi-photon entangled states. The robust propagation of multi-photon entangled states are crucial for applications in quantum information, computing and communications. Based on the corner state in the designed synthetic quadrupole topological insulator, the topologically protected entanglement between two, three and four photons states may be realized. To illustrate this effect, in the following, we focus on the quantum state composed of four photons, where the frequencies, OAMs and polarizations are entangled. The results for two and three photons are provided in the Supplementary Information. The single photon state should be selected at four corners in the synthetic space that are φ_0 ($l=10$ $n=-5$ $\theta=0$), φ_{45} ($l=10$ $n=5$ $\theta=45$), φ_{90} ($l=0$ $n=5$ $\theta=90$) and φ_{135} ($l=0$ $n=-5$ $\theta=135$). In this case, as an example, the input entangled four photons state can be expressed as:

$$|\psi\rangle = \frac{1}{\sqrt{2}}(|1_{\varphi_0}, 2_{\varphi_{45}}, 3_{\varphi_{90}}, 4_{\varphi_{135}}\rangle + |1_{\varphi_{90}}, 2_{\varphi_{135}}, 3_{\varphi_0}, 4_{\varphi_{45}}\rangle). \quad (7)$$

In Fig. 4a, we plot the numerical result of the steady-state output photons state with “zero energy” excitation when the system parameters are the same as those used in Fig. 3c. It is clearly shown that the output mode of four photons are still located at the initial state at the corner of the synthetic space. Hence, the input entangled state is preserved. Moreover, when the significant disorders are introduced in this synthetic quadrupole topological phase ($g(\chi)$ are randomly selected ranging from 4(0.5) to 16(2) on different lattice sites), as shown in Fig. 4b, we find that the output modes of four photons are still positioned at four corners in the synthetic space. The configuration average (10 times) has been performed. Consequently, we note that the propagation of the entangled multi-photon state is robust with disorders within the synthetic quadrupole topological insulators.

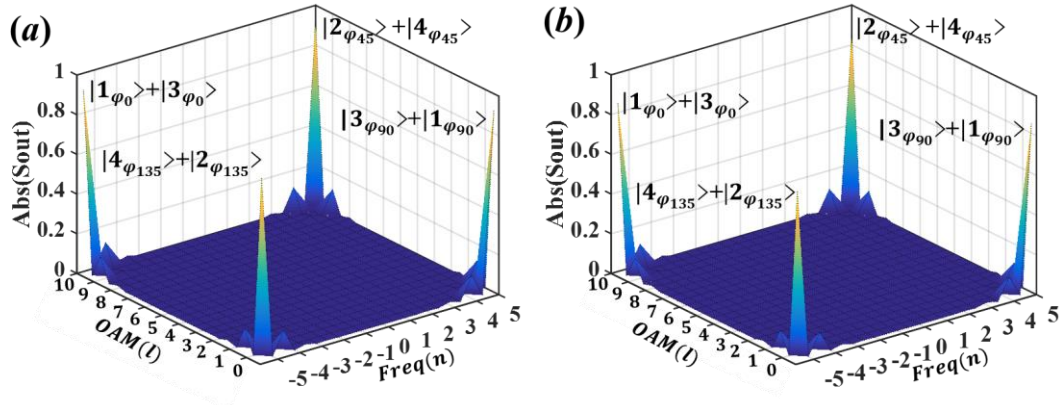


Figure 4 | Evolution of multi-photon entangled states with the excitation of synthetic corner state. (a) The steady-state solution of the output four photons state with the value of $g(\chi)$ being 8(1). (b) The steady-state modal distribution of output four photons state under the influence of disorder where $g(\chi)$ are randomly selected ranging from 4(0.5) to 16(2) on different lattice sites.

Discussion. Although the theoretical aspects of synthetic quadrupole topological insulator are only discussed in the present work, the designed 0D optical cavity with frequency, OAM and polarization control may be actually realized in experiments. In the free-space optics, we may let the central frequency ω_0 and the length of the optical cavity L to be 100THz and 1~10m, respectively. The modal spacing and modulation frequency of EOM are nearly ranging from 10 to 100MHz $\ll\omega_0$ ⁵¹. With this dense cavity modes distribution, the dispersion effect can be neglected for a large different frequencies of cavity modes. However, it is important to note that the losses in all optical elements can lead to a broadening of the cavity mode, which can make the dense cavity mode become undistinguishable. To solve this problem, we can placing an amplifier in the optical path to increase the quality factor of the cavity mode without lasing (decrease the linewidth of the cavity mode). On the other hand, to realize the non-trivial coupling conditions ($g=\kappa>\chi$), the reflectivities of ‘BS_A’ and

‘BS_B’ should be suitably tuned to satisfy the relationship of $b=\beta/(1+\beta)>0.5a/(1-a)$. In our weak modulation range $\beta\ll 1$, the reflectivities of ‘BS_A’ and ‘BS_B’ are also needed to be low. Additionally, the required polarization and phase control can also be directly achieved using traditional optical elements, such as polarizer, liquid crystal retarder and quarter-wave plate. The most difficult procedure in our system is introducing “boundaries” in the synthetic space. We can follow the previous work to introduce the frequency boundary by coupling with a secondary cavity⁵¹. And, creating the OAM boundary by designing holes in BSs⁴⁵.

In conclusion, we have theoretically designed the first photonic quadrupole topological insulator in $2D$ synthetic spaces with the utilization of $0D$ optical cavities. The coupling between optical cavity modes with different frequencies, OAMs and polarizations are used to fulfill the corresponding tight-binding lattice model in the synthetic space. The numerical results based on the coupled-mode theory demonstrated that the steady-state solution at “zero energy” of the output field from the synthetic quadrupole topological insulator is totally located at the corner of the $2D$ synthetic spaces even if significant disorders exist. By using the robust corner state in the synthetic spaces, the topological protection of multi-photon entangled state is proved. Our designed synthetic photonic quadrupole topological insulators propose a unique platform to explore higher-order topological photonics and offer possibilities for robust shaping of light in synthetic dimensions.

References

1. Hasan, M. Z. & Kane, C. L. Colloquium: Topological insulators, *Rev. Mod. Phys.* **82**, 3045–3067 (2010).
2. Qi, X. L. & Zhang, S. C. Topological insulators and superconductors, *Rev. Mod. Phys.* **83**, 1057–1110 (2011).
3. Lu, L., Joannopoulos, J. D. & Soljačić, M. Topological photonics, *Nat. Photonics* **8**, 821-829 (2014).

4. Ozawa, T., Price, H. M., Amo, A., Goldman, N., Hafezi, M., Lu, L., Rechtsman, M. C., Schuster, D., Zilberberg, O. & Carusotto, L. Topological photonics, *Rev. Mod. Phys.* **91**, 015006 (2019).
5. Khanikaev, A.B. & Shvets, G. Two-dimensional topological photonics, *Nat. Photonics* **11**, 763-773 (2017).
6. Ma, G., Meng, X. & Chan, C. T. Topological phases in acoustic and mechanical systems, *Nat. Rev. Phys.* **1**, 281-294 (2019).
7. Su, W. P., Schrieffer, J. R. & Heeger, A. J. Solitons in polyacetylene, *Phys. Rev. Lett.* **42**, 1698-1701 (1979).
8. Meng, X., Zhang, Z. Q. & Chan, C. T. Surface impedance and bulk band geometric phases in one-dimensional systems, *Phys. Rev. X* **4**, 021017 (2014).
9. Blanco-Redondo, A., Andonegui, I., Collins, M. J., Harari, G., Lumer, Y., Rechtsman, M.C., Eggleton, B. J. & Segev, M. Topological optical waveguiding in silicon and the transition between topological and trivial defect states, *Phys. Rev. Lett.* **116**, 163901 (2016).
10. Slobozhanyuk, A. P., Poddubny, A. N., Miroshnichenko, A. E., Belov, P. A. & Kivshar, Y. S. Subwavelength topological edge states in optically resonant dielectric structures, *Phys. Rev. Lett.* **114**, 123901 (2015).
11. Zhang, W. & Zhang, X. Backscattering-Immune computing of spatial differentiation by nonreciprocal plasmonics, *Phys. Rev. Applied* **11**, 054003 (2019).
12. Poddubny, A., Miroshnichenko, A., Slobozhanyuk, A. & Kivshar, Y. S. Topological Majorana States in Zigzag Chains of Plasmonic Nanoparticles, *ACS Photonics* **3**, 1468 (2016).
13. Zhang, W., Wu, T. & Zhang, X. Reconfigurable topological phases in photoexcited graphene nanoribbon arrays, *J. Opt.* **20**, 095005 (2018).
14. Haldane, F. D. M. & Raghu, S. Possible realization of directional optical waveguides in photonic crystals with broken time-reversal symmetry, *Phys. Rev. Lett.* **100**, 013904 (2008).
15. Wang, Z., Chong, Y. D., Joannopoulos, J. D. & Soljačić, M. Observation of

- unidirectional backscattering-immune topological electromagnetic states, *Nature* **461**, 772-775 (2009).
16. Rechtsman, M. C., Zeuner, J. M., Plotnik, Y., Lumer, Y., Podolsky, D., Dreisow, F., Nolte, S., Segev, M. & Szameit, A. Photonic Floquet topological insulators, *Nature* **496**, 196-200 (2013).
 17. Fang, K., Yu, Z. & Fan, S. Realizing effective magnetic field for photons by controlling the phase of dynamic modulation, *Nat. Photonics* **6**, 782-787 (2012).
 18. Hafezi, M., Demler, E. A., Lukin, M. D. & Taylor, J. M. Robust optical delay lines with topological protection, *Nat. Phys.* **7**, 907-912 (2011).
 19. Khanikaev, A. B., Mousavi, S. H., Tse, W. K., Kargarian, M., MacDonald, A. H. & Shvets, G. Photonic topological insulators, *Nat. Mater.* **12**, 233-239 (2013).
 20. He, C., Sun, X. C., Liu, X. P., Lu, M. H., Chen, Y., Feng, L. & Chen, Y. F. Photonic topological insulators with broken time-reversal symmetry, *Proc. Natl. Acad. Sci.* **113**, 4924-4928 (2016).
 21. Wu, L. H. & Hu, X. Scheme for achieving a topological photonic crystal by using dielectric material, *Phys. Rev. Lett.* **114**, 223901 (2015).
 22. Hafezi, M., Mittal, S., Fan, J., Migdall, A. & Taylor, J. M. Imaging topological edge states in silicon photonics, *Nat. Photonics* **7**, 1001-1005 (2013).
 23. Zhang, F., Kane, C. L. & Mele, E. J. Surface State Magnetization and Chiral Edge States on Topological Insulators, *Phys. Rev. Lett.* **110**, 046404 (2013).
 24. Benalcazar, W. A., Bernevig, B. A. & Hughes, T. L. Quantized electric multipole insulators, *Science* **357**, 61 (2017).
 25. Benalcazar, W. A., Bernevig, B. A. & Hughes, T. L. Electric multipole moments, topological multipole moment pumping, and chiral hinge states in crystalline insulators, *Phys. Rev. B* **96**, 245115 (2017).
 26. Langbehn, J., Peng, Y., Trifunovic, L., Oppen, F. & Brouwer, P. W. Reflection-Symmetric Second-Order Topological Insulators and Superconductors, *Phys. Rev. Lett.* **119**, 246401 (2017).
 27. Schindler, F., Cook, A. M., Vergniory, M. G., Wang, Z., Parkin, S. S. P., Bernevig, B. A. & Neupert, T. Higher-order topological insulators, *Sci. Adv.* **4**, 0346 (2018).

28. Schindler, F., Wang, Z., Vergniory, M. G., Cook, A. M., Murani, A., Sengupta, S., Kasumov, A. Yu., Deblock, R., Jeon, S., Drozdov, I., Bouchiat, H., Guéron, S., Yazdani, A., Bernevig, B. A. & Neupert, T. Higher-order topology in bismuth, *Nat. Phys.* **14**, 918 (2018).
29. Song, Z., Fang, Z. & Fang, C. (d-2)-Dimensional Edge States of Rotation Symmetry Protected Topological States, *Phys. Rev. Lett.* **119**, 246402 (2017).
30. Ezawa, M. Higher-Order Topological Insulators and Semimetals on the Breathing Kagome and Pyrochlore Lattices, *Phys. Rev. Lett.* **120**, 026801 (2018).
31. Kunst, F. K., Miert, G. V. & Bergholtz, E. J. Lattice models with exactly solvable topological hinge and corner states, *Phys. Rev. B* **97**, 241405(R) (2017).
32. Ni, X., Weiner, M., Alù, A. & Khanikaev, A. B. Observation of higher-order topological acoustic states protected by generalized chiral symmetry, *Nat. Materials* **18**, 113-120 (2019).
33. Xue, H., Yang, Y., Gao, F., Chong, Y. & Zhang, B. Acoustic higher-order topological insulator on a kagome lattice, *Nat. Materials* **18**, 108-112 (2019).
34. Noh, J., Benalcazar, W. A., Huang, S., Collins, M. J., Chen, K. P., Hughes, T. L. & Rechtsman, M. C. Topological protection of photonic mid-gap defect modes, *Nat. Photonics* **12**, 408 (2018).
35. Xie, B.-Y., Wang, H.-F., Wang, H.-X., Zhu, X.-Y., Jiang, J.-H., Lu, M.-H. & Chen, Y.-F. Second-order photonic topological insulator with corner states, *Phys. Rev. B* **98**, 205147 (2018).
36. Peterson, C. W., Benalcazar, W. A., Hughes, T. L. & Bahl, G. A quantized microwave quadrupole insulator with topologically protected corner states, *Nature* **555**, 346 (2018).
37. Serra-Garcia, M., Peri, V., Süsstrunk, R., Bilal, O. R., Larsen, T., Villanueva, L. G. & Huber, S. D. Observation of a phononic quadrupole topological insulator, *Nature* **555**, 342 (2018).
38. Mittal, S., Orre, V. V., Zhu, G., Gorlach, M. A., Poddubny, A. & Hafezi, M. Photonic quadrupole topological phases, arXiv 1812.09304 (2018).
39. Imhof, S., Berger, C., Bayer, F., Brehm, J., Molenkamp, L. W., Kiessling, T.,

- Schindler, F., Lee, C. H., Greiter, M., Neupert, T. & Thomale, R. Topoelectrical-circuit realization of topological corner modes, *Nat. Phys.* **14**, 925 (2018).
40. Yuan, L., Lin, Q., Xiao, M. & Fan, S. Synthetic dimension in photonics, *Optica* **5**, 1396 (2018).
41. Yuan, L., Shi, Y. & Fan, S. Photonic gauge potential in a system with a synthetic frequency dimension, *Opt. Lett.* **41**, 741 (2016).
42. Ozawa, T., Price, H. M., Goldman, N., Zilberberg, O. & Carusotto, I. Synthetic dimensions in integrated photonics: From optical isolation to four-dimensional quantum Hall physics, *Phys. Rev. A* **93**, 043827 (2016).
43. Yuan, L., Xiao, M., Lin, Q., & Fan, S. Synthetic space with arbitrary dimensions in a few rings undergoing dynamic modulation, *Phys. Rev. B* **97**, 104105 (2018).
44. Luo, X.-W., Zhou, X., Xu, J.-S., Li, C.-F., Guo, G.-C., Zhang, C. & Zhou, Z.-W. Synthetic-lattice enabled all-optical devices based on orbital angular momentum of light, *Nat. Commun.* **8**, 16097 (2017).
45. Zhou, X.-F., Luo, X.-W., Wang, S., Guo, G.-C., Zhou, X., Pu, H., & Zhou, Z.-W. *Phys. Dynamically Manipulating Topological Physics and Edge Modes in a Single Degenerate Optical Cavity*, *Rev. Lett.* **118**, 083603 (2017).
46. Kraus, Y. E., Lahini, Y., Ringel, Z., Verbin, M. & Zilberberg, O. Topological states and adiabatic pumping in quasicrystals, *Phys. Rev. Lett.* **109**, 106402 (2012).
47. Verbin, M., Zilberberg, O., Kraus, Y. E., Lahini, Y. & Silberberg, Y. Observation of topological phase transitions in photonic quasicrystals, *Phys. Rev. Lett.* **110**, 076403 (2013).
48. Zilberberg, O., Huang, S., Guglielmon, J., Wang, M., Chen, K. P., Kraus, Y. E. & Rechtsman, M. C. Photonic topological boundary pumping as a probe of 4D quantum Hall physics, *Nature* **553**, 59–62 (2018).
49. Wang, Q., Xiao, M., Liu, H., Zhu, S. & Chan, C. T. Optical interface states protected by synthetic Weyl points, *Phys. Rev. X* **7**, 031032 (2017).
50. Yuan, L. & Fan, S. Bloch oscillation and unidirectional translation of frequency in a dynamically modulated ring resonator, *Optica* **3**, 1014–1018 (2016).

51. Yuan, L., Lin, Q., Zhang, A., Meng, X., Chen, X. & Fan, S. Photonic Gauge Potential in One Cavity with Synthetic Frequency and Orbital Angular Momentum Dimensions, *Phys. Rev. Lett.* **122**, 083903 (2019).
52. Lin, Q., Xiao, M., Yuan, L. & Fan, S. Photonic Weyl point in a two-dimensional resonator lattice with a synthetic frequency dimension, *Nat. Commun.* **7**, 13731 (2016).
53. Lin, Q., Sun, X.-Q., Xiao, M., Zhang, S.-C. & Fan, S. Constructing three-dimensional photonic topological insulator using two-dimensional ring resonator lattice with a synthetic frequency dimension, arXiv: 1802.02597 (2018).
54. Lustig, E., Weimann, S., Plotnik, Y., Lumer, Y., Bandres, M. A., Szameit, A. & Segev, M. Photonic topological insulator in synthetic dimensions, *Nature* **567**, 356-360 (2019).

Acknowledgements

This work was supported by the National key R&D Program of China under Grant No. 2017YFA0303800 and the National Natural Science Foundation of China through Grants No. 91850205 and No.61421001.

Supporting Information

Photonic Quadrupole Topological phases in Zero-Dimensional Cavity with Synthetic Dimensions

Weixuan Zhang^{1,2} and Xiangdong Zhang^{1,2*}

¹Key Laboratory of advanced optoelectronic quantum architecture and measurements of Ministry of Education,
School of Physics, Beijing Institute of Technology, 100081, Beijing, China;

²Beijing Key Laboratory of Nanophotonics & Ultrafine Optoelectronic Systems, Micro-nano Center, School of
Physics, Beijing Institute of Technology, 100081, Beijing, China;

*Corresponding author, E-Mail address: zhangxd@bit.edu.cn

S1: The steady-state output solution with the input polarization angle being 45deg, 90deg and 135deg.

In this part, we consider the steady-state output solution with the input polarization angle being 45deg, 90deg and 135deg, respectively. The structural parameters used here are the same with the result in Fig. 3(c). When the incident signal is $S_{10,5,45}^{in} = 1$, the general coupled-mode equations can be expressed as:

$$\begin{aligned}\frac{dc_{l,n,0}}{dt} &= -\gamma c_{l,n,0} - i\chi c_{l,n,45} + i\chi c_{l,n,135} - igc_{l,n-1,45}(1-\delta_{-5,n}) - i\kappa c_{l+1,n,135}(1-\delta_{10,l}) \\ \frac{dc_{l,n,45}}{dt} &= -\gamma c_{l,n,45} - i\chi c_{l,n,0} - i\chi c_{l,n,90} - igc_{l,n+1,0}(1-\delta_{5,n}) - i\kappa c_{l+1,n,90}(1-\delta_{10,l}) + \sqrt{\gamma} S_{10,5,45}^{in} \\ \frac{dc_{l,n,90}}{dt} &= -\gamma c_{l,n,90} - i\chi c_{l,n,45} - i\chi c_{l,n,135} - igc_{l,n+1,135}(1-\delta_{5,n}) - i\kappa c_{l-1,n,45}(1-\delta_{0,l}) \\ \frac{dc_{l,n,135}}{dt} &= -\gamma c_{l,n,135} - i\chi c_{l,n,90} + i\chi c_{l,n,0} - igc_{l,n-1,90}(1-\delta_{-5,n}) - i\kappa c_{l-1,n,0}(1-\delta_{0,l}) \\ S_{l,n,\theta}^{out} &= \sqrt{\gamma} c_{l,n,\theta}\end{aligned}\quad (S1)$$

Fig. S1(a) plots the corresponding steady-state solution. It is clearly shown that the output cavity modes are located at the corner of the synthetic space. The results with the input signal being $S_{0,5,90}^{in} = 1$ and $S_{0,-5,135}^{in} = 1$ are presented in Fig. S1(b) and S1(c), respectively. The corresponding coupled-mode equations can be expressed as:

$$\begin{aligned}\frac{dc_{l,n,0}}{dt} &= -\gamma c_{l,n,0} - i\chi c_{l,n,45} + i\chi c_{l,n,135} - igc_{l,n-1,45}(1-\delta_{-5,n}) - i\kappa c_{l+1,n,135}(1-\delta_{10,l}) \\ \frac{dc_{l,n,45}}{dt} &= -\gamma c_{l,n,45} - i\chi c_{l,n,0} - i\chi c_{l,n,90} - igc_{l,n+1,0}(1-\delta_{5,n}) - i\kappa c_{l+1,n,90}(1-\delta_{10,l}) \\ \frac{dc_{l,n,90}}{dt} &= -\gamma c_{l,n,90} - i\chi c_{l,n,45} - i\chi c_{l,n,135} - igc_{l,n+1,135}(1-\delta_{5,n}) - i\kappa c_{l-1,n,45}(1-\delta_{0,l}) + \sqrt{\gamma} S_{0,5,90}^{in}\end{aligned}\quad (\text{S2})$$

$$\begin{aligned}\frac{dc_{l,n,135}}{dt} &= -\gamma c_{l,n,135} - i\chi c_{l,n,90} + i\chi c_{l,n,0} - igc_{l,n-1,90}(1-\delta_{-5,n}) - i\kappa c_{l-1,n,0}(1-\delta_{0,l}) \\ S_{l,n,\theta}^{out} &= \sqrt{\gamma} c_{l,n,\theta} \\ \frac{dc_{l,n,0}}{dt} &= -\gamma c_{l,n,0} - i\chi c_{l,n,45} + i\chi c_{l,n,135} - igc_{l,n-1,45}(1-\delta_{-5,n}) - i\kappa c_{l+1,n,135}(1-\delta_{10,l}) \\ \frac{dc_{l,n,45}}{dt} &= -\gamma c_{l,n,45} - i\chi c_{l,n,0} - i\chi c_{l,n,90} - igc_{l,n+1,0}(1-\delta_{5,n}) - i\kappa c_{l+1,n,90}(1-\delta_{10,l}) \\ \frac{dc_{l,n,90}}{dt} &= -\gamma c_{l,n,90} - i\chi c_{l,n,45} - i\chi c_{l,n,135} - igc_{l,n+1,135}(1-\delta_{5,n}) - i\kappa c_{l-1,n,45}(1-\delta_{0,l}) \\ \frac{dc_{l,n,135}}{dt} &= -\gamma c_{l,n,135} - i\chi c_{l,n,90} + i\chi c_{l,n,0} - igc_{l,n-1,90}(1-\delta_{-5,n}) - i\kappa c_{l-1,n,0}(1-\delta_{0,l}) + \sqrt{\gamma} S_{0,-5,135}^{in} \\ S_{l,n,\theta}^{out} &= \sqrt{\gamma} c_{l,n,\theta}\end{aligned}\quad (\text{S3})$$

We find that the output fields are always located at the corner of the synthetic space. These phenomena are complete consistent with the property of corner state in the synthetic quadrupole topological insulators.

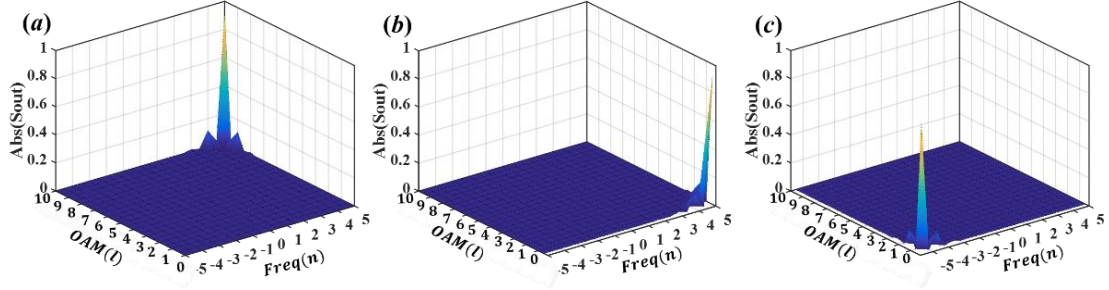


FIG. S1 (a)-(c) The steady-state modal distribution with the input signal being $S_{10,5,45}^{in} = 1$, $S_{10,-5,90}^{in} = 1$ and $S_{0,-5,135}^{in} = 1$, respectively.

S2: The steady-state output solution of the trivial insulator and the input signal locates in the bulk of synthetic spaces.

For comparison with the system with topologically non-trivial bulk band gap, in Figs. S2(a) and 2(b), we plot the output steady-state modal distribution with the value of $g(\chi)$ being 1(2) and 1(5), respectively. In this case, the intra-cell coupling is larger than the inter-cell coupling in the synthetic lattice model, and the system becomes a trivial insulator without

corner or edge state in the band gap. The used input signal is selected as $S_{10,-5.0}^{in} = e^{i0t}$. It is clearly shown that the localized output cavity modes in the synthetic space also exists. While, this localization is only resulting from the bulk band gap effect (the output modal pattern is different from the midgap corner state), and no topologically induced corner state can be excited.

In the following, we calculate the steady-state output solution when the input state is located in the bulk of synthetic spaces $S_{2,-3.0}^{in} = e^{i0t}$. Figs. S2(c) and S2(d) represent the corresponding steady-state modal distribution with the value of $g(\chi)$ being 1(1) and 2(1), respectively. We find that the extended modal distribution in the synthetic space appears with $g/\chi=1$ due to the corresponding gapless bulk band. When the value of g/χ gets increased, the bulk band gap opens. In this case, the output modes are localized near the source since the energy is in the bulk band gap.

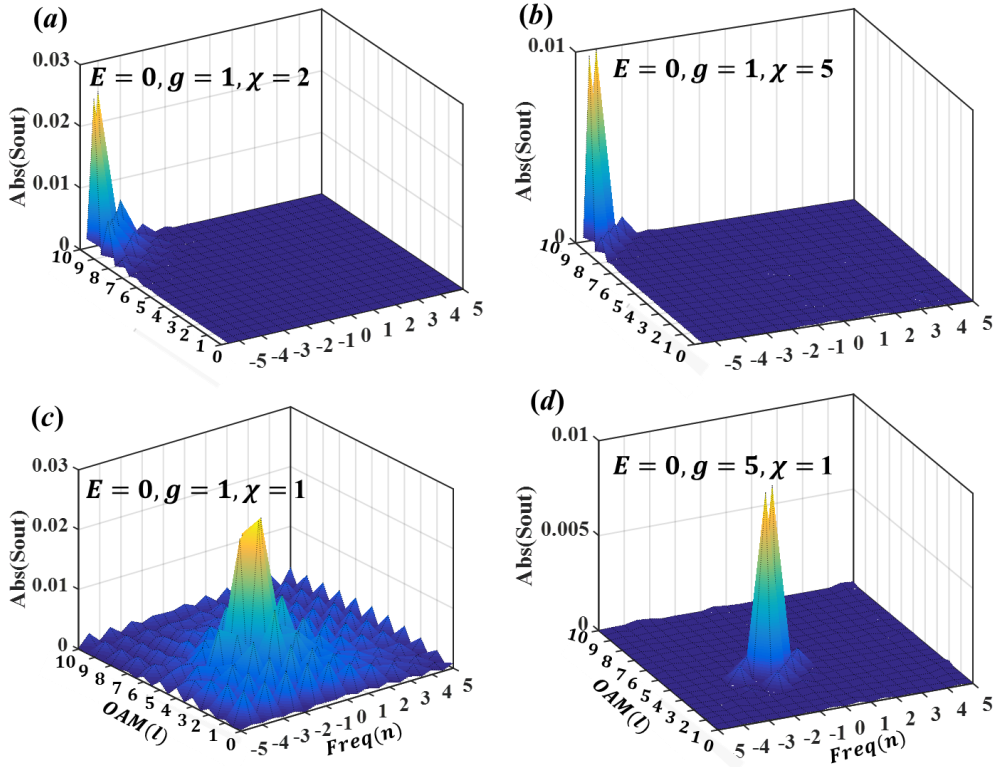


FIG. S2 (a) and (b) The steady-state modal distribution with the value of $g(\chi)$ being 1(2) and 1(5), respectively. The input mode is selected as $S_{10,-5.0}^{in} = 1$. (c) and (d) The steady-state modal distribution with the value of $g(\chi)$ being 1(1) and 2(1), respectively. The input mode being selected as $S_{2,-3.0}^{in} = e^{i0t}$.

S3: The steady-state output solution with the excitation of edge state.

Here, we calculate the steady-state modal distribution with the input mode being $S_{10,-5,0}^{in} = e^{i8t}$. In this case, according to the eigenspectrum shown in Fig. 2(b), the edge state in the synthetic space can be excited. This can be clearly seen in Fig. S3(a) where the output cavity modes are completely located at the edges of the synthetic space. On contrary to the corner state, the excited edge state is significantly disturbed by the disorder, as shown in Fig. S3(b).

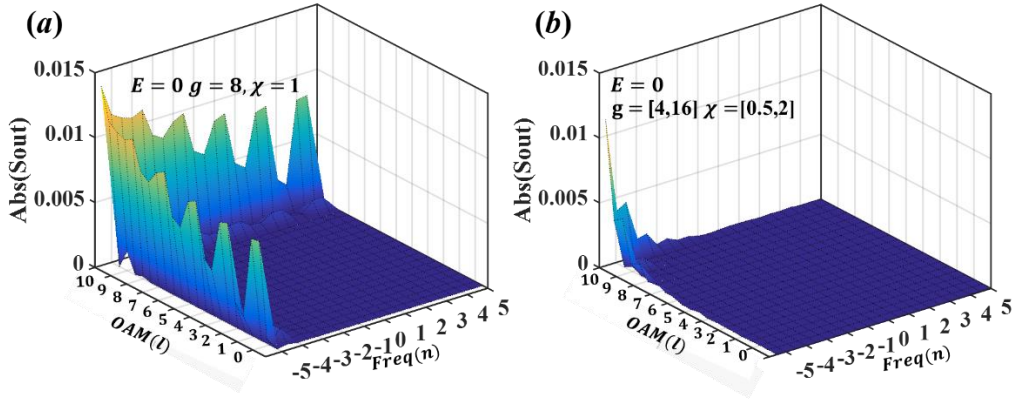


FIG. S3 (a) The steady-state modal distribution with the value of $g(\chi)$ being 1(8). (b) The steady-state modal distribution of edge state under the influence of disorder where $g(\chi)$ is randomly selected ranging from 4(0.5) to 16(2). The input mode is selected as $S_{10,-5,0}^{in} = e^{i8t}$.

S4: The topological protection of entangled two and three photons states.

In this part, we focus on the quantum state with two and three entangled photons. The corresponding input entangled states, as an example, can be expressed as:

$$\begin{aligned}
 |\psi\rangle &= \frac{1}{\sqrt{2}} (|1_{\varphi_0}, 2_{\varphi_{90}}\rangle + |1_{\varphi_{90}}, 2_{\varphi_0}\rangle) \\
 |\psi\rangle &= \frac{1}{\sqrt{2}} (|1_{\varphi_0}, 2_{\varphi_{90}}, 3_{\varphi_{45}}\rangle + |1_{\varphi_{90}}, 2_{\varphi_{45}}, 3_{\varphi_0}\rangle)
 \end{aligned} \tag{S3}$$

In Figs. S4(a) and 4(b), we plot the numerical results of the output photons state with “zero energy” excitation. We find that the output state of two or three photons are mainly located at the corner of the synthetic space. Hence, the input entangled states are preserved. When the significant disorders are introduced [$g(\chi)$ are randomly selected ranging from 4(0.5) to 16(2) between different lattice sites], the output modes of two and three photons are still positioned at corners in the synthetic space, as shown in Figs. S3(c) and S3(d). The configuration

average (10 times) is also performed. In this case, the propagation of the entangled two and three photons states is robust with disorders in our designed synthetic quadrupole topological insulators.

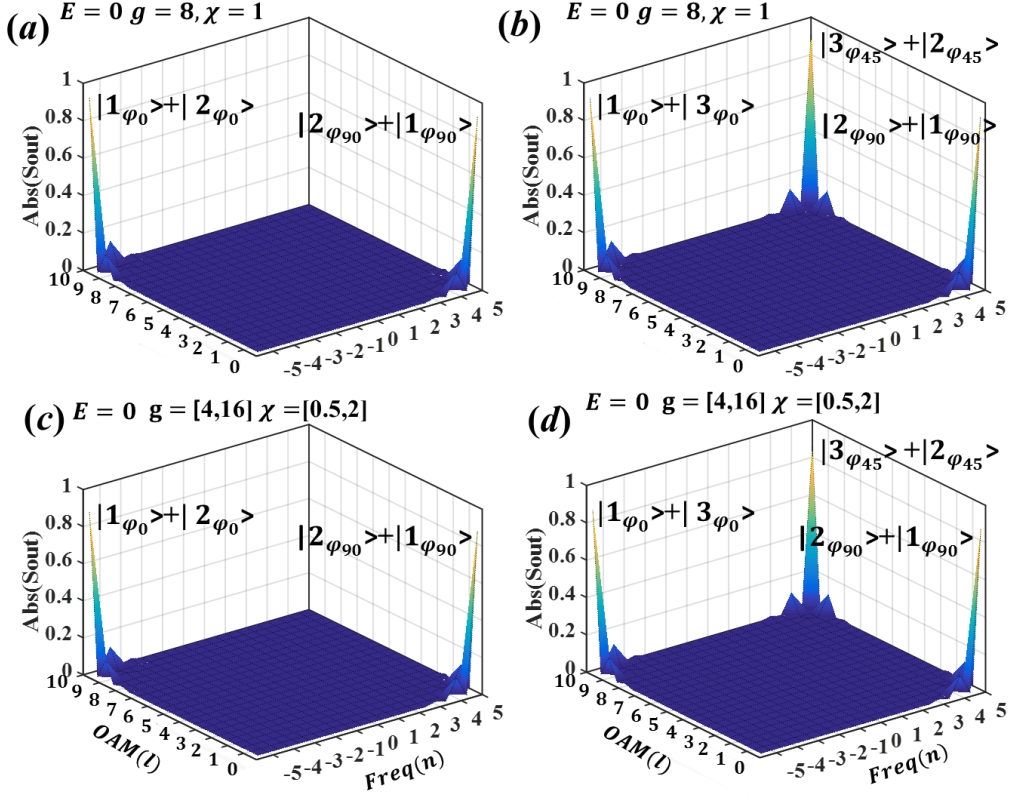


FIG. S4 (a) and (b) The steady-state solution of the output two and three photons states with the value of $g(\chi)$ being 8(1). (c) and (d) The steady-state modal distribution of output two and three photons states under the influence of disorder where $g(\chi)$ are randomly selected ranging from 4(0.5) to 16(2) between different lattice sites.